Guo *et al.*
Chinese Journal of Mechanical Engineering (2023) 36:105
https://doi.org/10.1186/s10033-023-00934-1

Chinese Journal of Mechanical Engineering

ORIGINAL ARTICLE

Open Access

Configuration Synthesis and Lightweight Networking of Deployable Mechanism Based on a Novel Pyramid Module

Jinwei Guo[1], Jianliang He[1], Guoxing Zhang[1], Yongsheng Zhao[2,3] and Yundou Xu[2,3*]

Abstract

Deployable mechanism with preferable deployable performance, strong expansibility, and lightweight has attracted much attention because of their potential in aerospace. A basic deployable pyramid unit with good deployability and expandability is proposed to construct a sizeable deployable mechanism. Firstly, the basic unit folding principle and expansion method is proposed. The configuration synthesis method of adding constraint chains of spatial closed-loop mechanism is used to synthesize the basic unit. Then, the degree of freedom of the basic unit is analyzed using the screw theory and the link dismantling method. Next, the three-dimensional models of the pyramid unit, expansion unit, and array unit are established, and the folding motion simulation analysis is carried out. Based on the number of components, weight reduction rate, and deployable rate, the performance characteristics of the three types of mechanisms are described in detail. Finally, prototypes of the pyramid unit, combination unit, and expansion unit are developed to verify further the correctness of the configuration synthesis based on the pyramid. The proposed deployable mechanism provides aference for the design and application of antennas with a large aperture, high deployable rate, and lightweight. It has a good application prospect in the aerospace field.

Keywords Pyramid unit, Deployable mechanism, Configuration synthesis, Structural design, Lightweight networking

1 Introduction

As one of the cutting-edge technologies in the international aerospace field, space-deployable structures have become an advanced research topic in space science and technology. Over the years, the critical technologies of space deployable structures have made breakthroughs in deployable mechanisms, cable membrane form finding, dynamic analysis, reliable environmental adaptability analysis, and verification [1]. With the development of communication, remote sensing, and navigation satellites, the research on deployable structure technology with large space antennas as the primary research object has attracted much attention. Researchers have paid significant interest to signal harvesters' equipment [2, 3]. Space deployable antenna mechanism is the critical equipment to support large-scale space antenna. With the characteristics of occupying a small space with a folding pose in the storage and launch stage and then gradually expanding when entering orbit, the antenna has high gain and high efficiency. Its development trend is large-scale, lightweight, and high deployable rate [4–7]. As an essential type of space deployable antenna, the truss deployable antenna mechanism has been successfully applied in the aerospace field with the advantages of good structural stability and high deployable rate. Typical

*Correspondence:
Yundou Xu
ydxu@ysu.edu.cn
[1] School of Mechanical Engineering, Jiangsu University of Science and Technology, Zhenjiang 212100, China
[2] Parallel Robot and Mechatronic System Laboratory of Hebei Province, Yanshan University, Qinhuangdao 066004, China
[3] Key Laboratory of Advanced Forging and Stamping Technology and Science of Ministry of National Education, Yanshan University, Qinhuangdao 066004, China

applications in China are the Beidou-3 satellite [8] and the HJ-1C satellite [9].

The deployable characteristic of the deployable mechanism is the premise of realizing a large unfolding rate. High enough stiffness and stability are the guarantees of supporting the antenna reflector, and the effective combination of large aperture and lightweight is the goal of mechanism design. The deployable mechanism is different from the general series/parallel mechanisms. It is a spatial multi-closed-loop mechanism composed of multiple basic units. Therefore, the basic unit configuration and deployable method of the deployable mechanism that meets the above characteristics still need to be continuously explored. For example, Phocas et al. [10] studied a reconfigurable and deployable linkage mechanism applied to the construction field. Sun et al. [11] studied a ring mesh deployable antenna mechanism based on H-shaped deployable units. Chen et al. [12] demonstrated the deployable mechanism design and networking method based on the classical linkage Bennett. Hofmann et al. [13] conducted design research on the positioner of the deployable spacecraft mechanism. In addition, many scholars have also focused on the design and research of spatial deployable units. Meng et al. [14] proposed a new basic unit with good composability and deployability, and thus constructed a double-layer ring deployable antenna mechanism and a variety of truss array deployable mechanisms. Yang et al. [15] studied a new type of deployable mechanism loaded with composite belt springs, which promoted the application of this type of mechanism in aerospace. Chen et al. [16] proposed a high-stiffness modular planar deployable antenna mechanism. Guo et al. [17] designed a deployable support mechanism for a space planar antenna. Lyu et al. [18] developed an isosceles trapezoidal prism deployable unit, and proposed a construction method using this unit to approximate a smooth plane curve or cylinder. Further, Wang et al. [19] proposed a design method of surface deployable mechanism, which takes the idea that the crease circumference is distributed around the central hub of the regular polygon as the design idea. Takamatsu et al. [20] proposed the concept configuration and construction mode of a deployable truss for a large antenna. Tian et al. [21] innovatively designed a networking method for a rib module and its large-size modular deployable antenna mechanism. Wang et al. [22] proposed a joint transformation configuration synthesis method, and innovatively designed a petal-type spatial deployable mechanism. Huang et al. [23, 24] developed a petal-type deployable mechanism and its improved mechanism. Both mechanisms have good packaging ratios and deployable performance, but the improved mechanism has a simple structure and good mechanical properties. What's more, Wu et al. [25] studied the nonlinear response of a flexible deployable linkage using the finite particle method. Zhang et al. [26] proposed a new type of hybrid antenna-supporting mechanism and analyzed its motion characteristics. In terms of the research on truss mechanisms, Xu et al. [27] proposed a space multi-loop mechanism configuration synthesis method with constraint chains, synthesized a variety of tetrahedral deployable units suitable for parabolic truss deployable antenna mechanism, and designed a large aperture antenna networking mode. Based on this, Guo et al. [28–30] proposed a modular tetrahedral truss deployable antenna mechanism and studied its mechanical properties, structural design, and comprehensive performance. The above literature offers various deployable unit mechanisms with excellent performance, and some deployable antenna mechanisms can be networked and applied to aerospace, but there are problems such as insufficient deployable rate and unsatisfactory scalability. Consequently, exploring more new types of deployable mechanisms and networking methods has intense academic research significance.

To obtain a high-performance deployable antenna mechanism, the optimization design of a deployable antenna mechanism is the effective way, especially the optimization design aiming at structural lightweight. Kim et al. [31] proposed a lightweight reconfigurable deformable origami block mechanism, which can be used as a driver to realize fast, reversible, and stable movement. Ze et al. [32] proposed a reversible wireless deployable microrobot. Sofla et al. [33] studied a single degree of freedom(DOF) articulated tetrahedral truss mechanism, and optimized a deformable articulated truss structure through two different tetrahedral arrangement modes. Dai et al. [34] used a genetic algorithm and gradient-based optimizer to optimize the overall structure and component size of a new double-ring deployable antenna mechanism. Further, Dai et al. [35] optimized the link size of the double-ring deployable antenna mechanism under the target of high stiffness and lightweight based on the constraints of dynamic characteristics. Wang et al. [36] studied a spatial cylindrical deployable structure with a large unfolding ratio and few DOFs inspired by Kirigami. They proposed an optimal design method of cylindrical deployable structure parameters that is most suitable for the target surface. Xu et al. [37] proposed a configuration optimization method of a parallel mechanism with few kinematic joints, two rotations, and one shift, based on the limit constraint screw, and constructed a five-axis hybrid robot with the most miniature kinematic joints. Mei et al. [38] applied the lightweight design concept to the parallel mechanism and proposed a lightweight and highly flexible five-axis mobile processing robot.

The above literature has proposed various mechanism optimization design methods to achieve mechanism lightweight. Still, there are few reports on the effective lightweight design methods of truss deployable antenna mechanisms.

Deployable mechanisms are mostly complex multi-closed-loop mechanisms, which are problematic in configuration synthesis, motion analysis, lightweight design, and experimental research. It is significant to explore the spatial multi-loop coupling deployable mechanism with a high deployable rate, strong scalability, and light structure. This paper focuses on the design and analysis of a deployable mechanism based on a pyramid unit, which is extensible and lightweight. In the second section, a new type of pyramid deployable unit mechanism and its configuration synthesis method are proposed. In the third section, the motion characteristics of the pyramid deployable unit are analyzed. In the fourth section, the structure design and motion simulation analysis of the deployable mechanism based on the pyramid unit is carried out, and the principal prototypes are developed to complete the experiment.

2 Configuration Synthesis of Deployable Pyramid Mechanism

Based on the configuration synthesis method with adding constraint chain of spatial closed-loop mechanism, the synthesis process of pyramid deployable unit mechanism includes the determination of the folding principle, the design of constraint chains, the addition of virtual constraint chains, and the construction of mechanisms. The configuration synthesis flow chart is shown in Figure 1.

2.1 Folding Principle of the Basic Deployable Unit

The large antenna reflector is mainly composed of several basic geometric units, including triangle, quadrilateral, pentagon, and other elemental planes. This paper studies a new deployable antenna reflector networking method and its supporting mechanism from the geometric units that constitute the hexagonal combination unit. As shown in Figure 2, three rectangles are circularly arrayed, and the boundary vertices are connected to form a hexagonal multi-closed-loop unit, that is, the hexagonal unit division based on quadrilateral. Then, the hexagonal multi-closed-loop unit is expanded by the mode of common boundary connection.

The aggregation principle of quadrilateral units is shown in Figure 3. The quadrilateral is a rectangle with two equal sides, namely AB=CD, and AD=BC, and its center point O is the circumscribed circle center of the quadrilateral $ABCD$. The expected movement of the four nodes of the quadrilateral is to move towards the center O, and the distance between the nodes gradually decreases, and finally converges near the target axis. According to the principle of unit convergence, a translational joint (P) can be used between each node and the center of its quadrilateral to describe the motion characteristics of the node. To ensure the synchronization of the folding movement of the unit, the four nodes should be close to the center point at the same time, so the side length of the quadrilateral changes proportionally at any time, that is, $A\prime B\prime / AB = B\prime C\prime / BC = C\prime D\prime / CD = A\prime D\prime / AD = \lambda$, λ is a constant.

2.2 Constraint Chain Synthesis of the Basic Unit

According to the folding principle of a quadrilateral node, only the distance between the four nodes A, B, C, and D

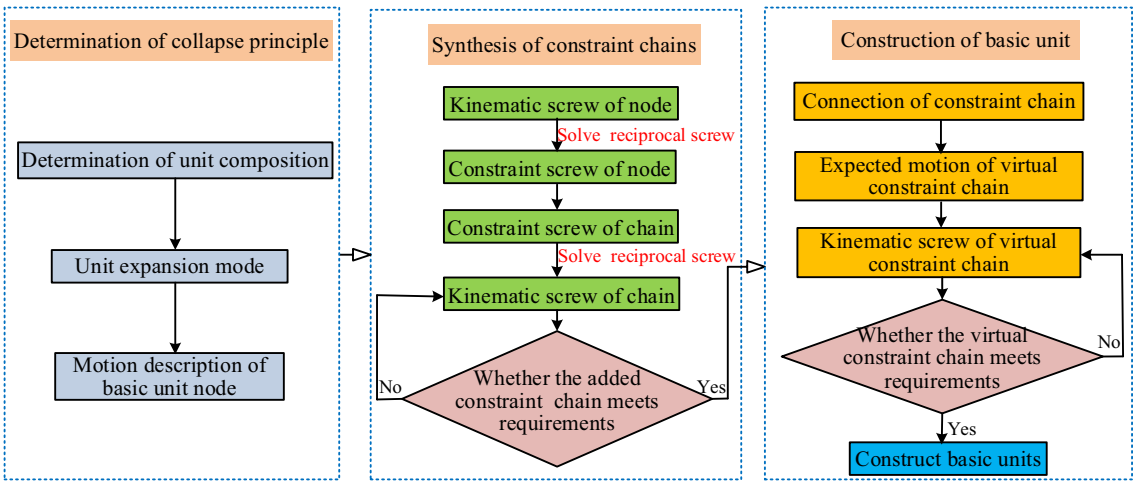

Figure 1 Configuration synthesis flow chart of pyramid mechanism

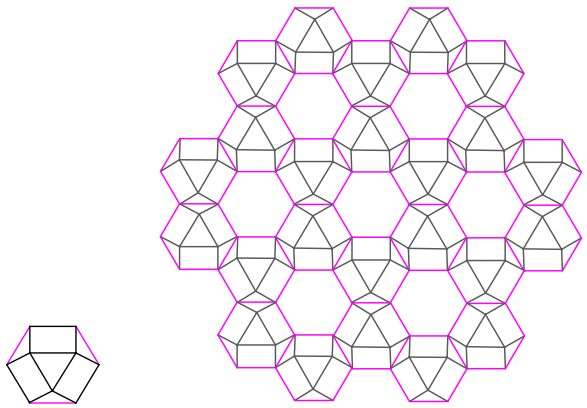

Figure 2 The hexagon unit and its expansion mode

changes, and the direction of movement and deployable between adjacent nodes remains the same, always along the line direction of the two nodes at the initial position. Therefore, it is necessary to add a constraint chain between two adjacent floral nodes that can move in this direction, so that it can follow the motion of the node, and can structurally limit the relative movement of the two floral nodes. It is assumed that the four nodes are folding to the target axis through a P joint. After adding the constraint chain between the two adjacent nodes, the constraint chain and the two P joints form a closed loop, which can be regarded as a parallel mechanism composed of two chains. For example, a constraint chain is added between nodes A and D, as shown in Figure 4.

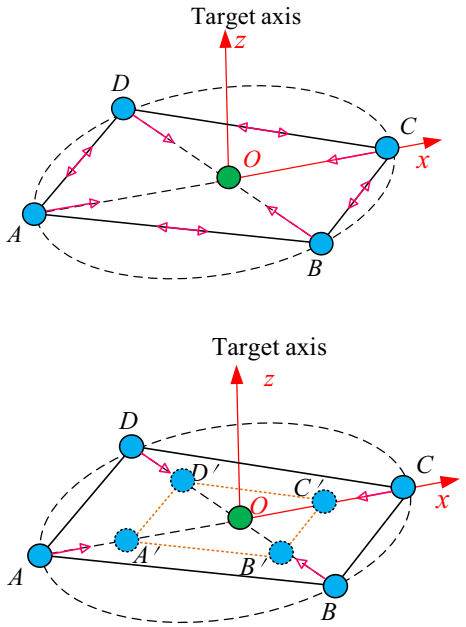

Figure 3 Node motion of the quadrilateral unit

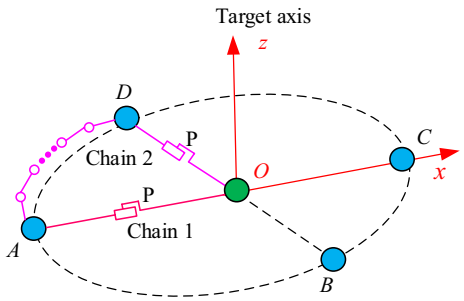

Figure 4 Constraint chains between adjacent nodes

The P joint connected with node A is regarded as constraint chain 1, and the P joint and constraint chain connected with node D is regarded as constraint chain 2, and nodes O and A are fixed and moving platforms respectively. According to the requirements of node motion, the closed-loop mechanism should have only one DOF.

As shown in Figure 4, a reference coordinate system O-xyz is established at the central node O, where the x-axis is along the diagonal AC, which is also the axis path of the P joint in the constraint chain 1, the z-axis is along the path of the target folding axis, the target axis is vertical to the quadrilateral plane, and the y-axis is determined by the right-hand rule. Then the kinematic screw of the P joint in constraint chain 1 can be expressed in O-xyz as:

$$\$^{\mathrm{m}} = \begin{pmatrix} 0 & 0 & 0 & 1 & 0 & 0 \end{pmatrix}. \tag{1}$$

Solving the reciprocal screw of Eq. (1) to obtain the constraint screw system imposed by the constraint chain 1 on node A as:

$$\$^{\mathrm{r}} = \begin{pmatrix} \$^{\mathrm{r}}_{11} \\ \$^{\mathrm{r}}_{12} \\ \$^{\mathrm{r}}_{13} \\ \$^{\mathrm{r}}_{14} \\ \$^{\mathrm{r}}_{15} \end{pmatrix} = \begin{pmatrix} 0 & 1 & 0 & 0 & 0 & 0 \\ 0 & 0 & 1 & 0 & 0 & 0 \\ 0 & 0 & 0 & 1 & 0 & 0 \\ 0 & 0 & 0 & 0 & 1 & 0 \\ 0 & 0 & 0 & 0 & 0 & 1 \end{pmatrix}. \tag{2}$$

Constraint chain 2 is formed by connecting the P joint connected with node A and the added constraint chain in series. To make the two constraint chain mechanisms have only one DOF, the maximum number of linearly independent motion joints of constraint chain 2 should be 6. The constraint screw provided by constraint chain 2 must be linearly related to the constraint screw system shown in Eq. (2), which can be 0–5 of the five constraint screws shown in Eq. (2). However, since the constraint chain 2 already contains a P joint, the constraint force axis provided by the constraint chain 2 must be perpendicular to the axis of the P joint, which $\$^{\mathrm{r}}_{11}$ cannot exist. Therefore, the constraint screw provided by the constraint chain 2 can only be 0–4 of $\$^{\mathrm{r}}_{12}$, $\$^{\mathrm{r}}_{13}$, $\$^{\mathrm{r}}_{14}$, and $\$^{\mathrm{r}}_{15}$. If constraint chain 2 does not provide constraints,

the added constraint chain can only provide a constraint force whose axis is not perpendicular to the P joint in constraint chain 2. At the same time, the constraint force should also ensure the synchronous movement of nodes *A* and *B*. Therefore, the constraint force is located in the plane perpendicular to the connecting line of nodes *A* and *B*, which is recorded as:

$$\$_{21}^{\mathrm{r}} = \left(s_1 \;\; s_2 \;\; s_3 \;\; bs_3 \;\; -as_3 \;\; as_2 - bs_1 \right), \tag{3}$$

where $\left(a \;\; b \;\; c \right)$ refers to any point on the axis of the constraint force $\$_{21}^{\mathrm{r}}$, and $\left(s_1 \;\; s_2 \;\; s_3 \right)$ refers to the axis direction of the $\$_{21}^{\mathrm{r}}$, where s_1 and s_2 cannot be zero at the same time.

According to the reciprocal screw theory, the constraint force/couple provided by the added constraint chain when constraint chain 2 provides 0–4 constraint screws, respectively, and the corresponding typical constraint chains are shown in Table 1.

Among all the constraint chains synthesized above, the P constraint chain and RRR constraint chain have the simplest structure. The quadrilateral mechanism formed by adding three P constraint chains and RRR constraint chains is shown in Figures 5 and 6, respectively. The constraint chain structurally restricts the synchronous movement of two adjacent nodes to the central node.

The quadrilateral deployable mechanism obtained by adding constraint chains is a planar mechanism in the entirely

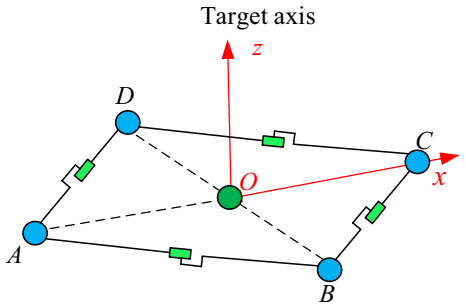

Figure 5 4P mechanism

Table 1 Typical constraint chains

Constraint force/couple provided by constraint chain 2	Constraint force/couple provided by added constraint chain	Typical constraint chains
None	One constraint force	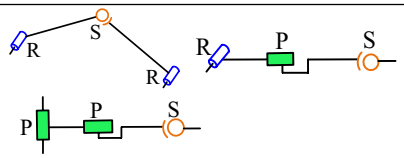
One constraint force	Two constraint forces	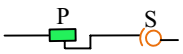
One constraint force and one constraint couple	Two constraint forces and one constraint couple	
One constraint force and two constraint couples	Two constraint forces and two constraint couples	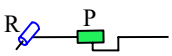
One constraint force and three constraint couples	Two constraint forces and three constraint couples	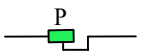
One constraint couple	One constraint force and one constraint couple	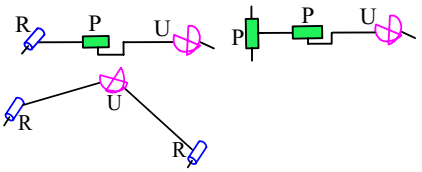
Two constraint couples	One constraint force and two constraint couples	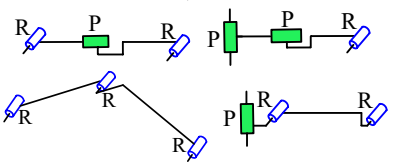
Three constraint couples	One constraint force and three constraint couples	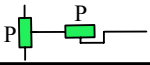

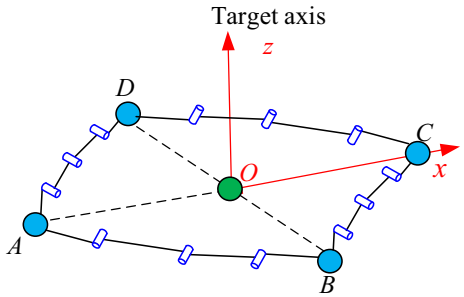

Figure 6 4RRR mechanism

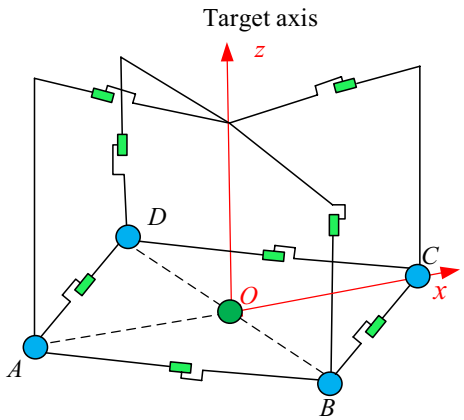

Figure 7 4P-4P mechanism

unfolding state, and its stiffness is low. Therefore, a virtual constraint chain can be added to improve the overall stiffness of the mechanism. Take node A as an example to illustrate, the added virtual constraint chain should be able to follow the movement of node A in the direction of AO. Therefore, the kinematic screw system of the virtual constraint chain should be composed of multiple (1–3) kinematic screws.

The synthesis results show that the virtual constraint chain with P joint and RR joints has the simplest structure of all virtual constraint chains that meet the requirements. The mechanisms formed by adding virtual constraint chain P and RR to Figures 5 and 6 are shown in Figures 7, 8, 9 and 10, respectively. The virtual constraint chain is used to make the position of the central slider precisely at the origin O.

Considering that the folding volume of the mechanism with the P joint is far smaller than that of the mechanism with only the R joint, the 4RRR-4RR quadrilateral mechanism composed of the RR virtual constraint chain and RRR constraint chain is preferred as the basic deployable unit mechanism of the truss antenna. Considering the expansion mode of the deployable antenna mechanism, the combination unit of the deployable antenna

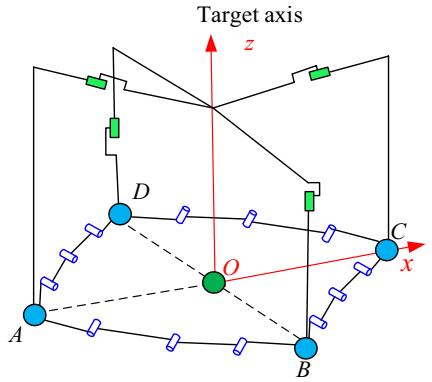

Figure 8 4RRR-4P mechanism

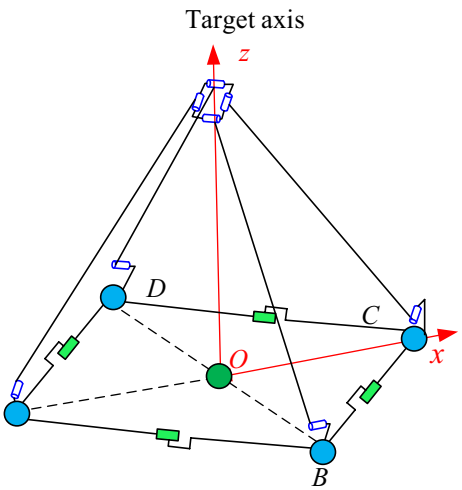

Figure 9 4P-4RR mechanism

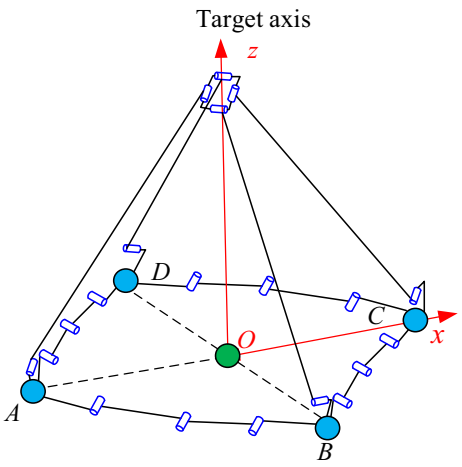

Figure 10 4RRR-4RR mechanism

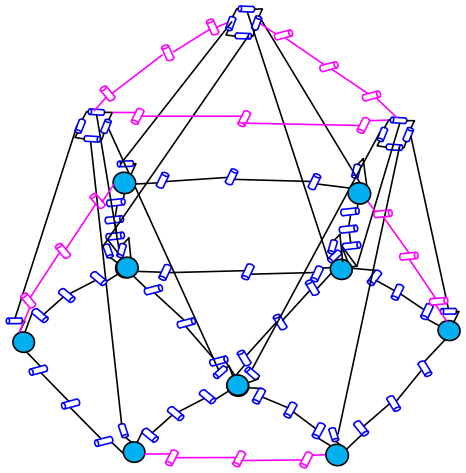

Figure 11 The combination unit based on three 4RRR-4RR pyramid units

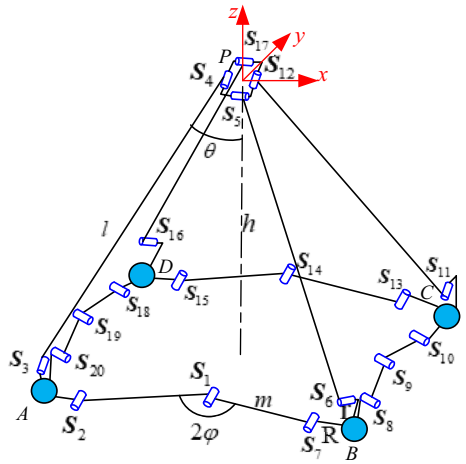

Figure 12 Schematic diagram of the 4RRR-4RR pyramid unit

mechanism can be obtained based on three 4RRR-4RR pyramid units, as shown in Figure 11.

3 Kinematic Characteristics Analysis of the Deployable Mechanism Based on 4RRR-4RR

In the 4RRR-4RR unit, the plane of the four revolute axes connected by the four webs and the top node, the three revolute auxiliary axes in the same synchronizing link are parallel to each other. The revolute axes in all synchronizing links are perpendicular to the connecting lines of the nodes at both ends of the synchronizing link, as shown in Figure 12. Establish a reference coordinate system *o-xyz* at the center of the top node *P*, the *z*-axis is vertical to the end face of the top node *P*, the *x*-axis is along the center line of the bottom node *A* and *C* and points from *A* to *C*, and the *y*-axis is determined according to the right-hand rule.

The 4RRR-4RR pyramid unit can be decomposed into a three-closed-loop mechanism and a RRR ($\boldsymbol{S}_{18}$, $\boldsymbol{S}_{19}$, and $\boldsymbol{S}_{20}$) kinematic chain, in which the three-closed-loop mechanism is composed of three 7R single closed-loop mechanisms sharing two webs, as shown in Figure 13.

Due to the symmetry of the structure, the RRR kinematic chain is a redundant constraint chain; that, it does not affect the DOF of the pyramid unit. Therefore, the DOF of the 4RRR-4RR pyramid unit is the same as that of the three-closed-loop mechanism. Next, the DOF of the three-closed-loop mechanism is analyzed. The structural diagram of the three-closed-loop mechanism and its topology diagram are shown in Figures 14 and 15, respectively.

The three-closed-loop mechanism can be regarded as a parallel mechanism, and the fixed platform (node *B*) and the moving platform (node *A*) are connected by two constraint chains. One is the RRR constraint chain ($\boldsymbol{S}_2$,

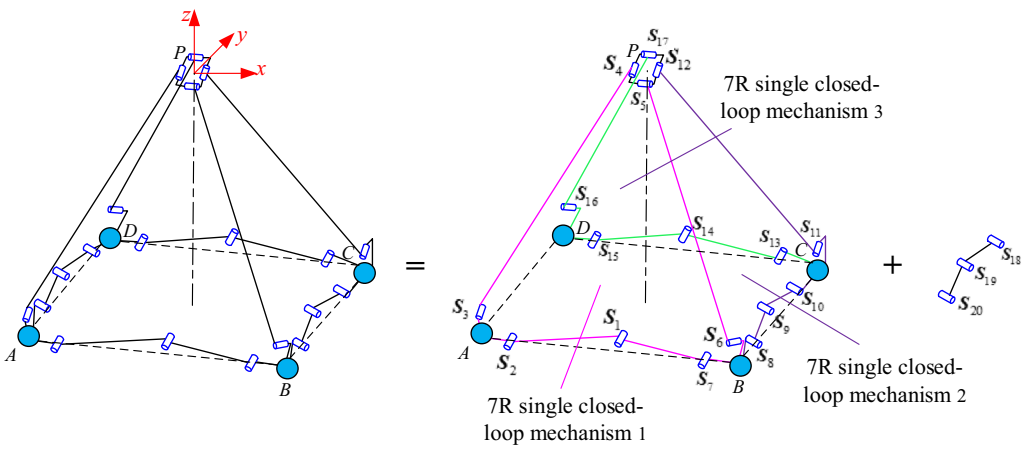

Figure 13 The equivalent splitting mechanism of the pyramid unit

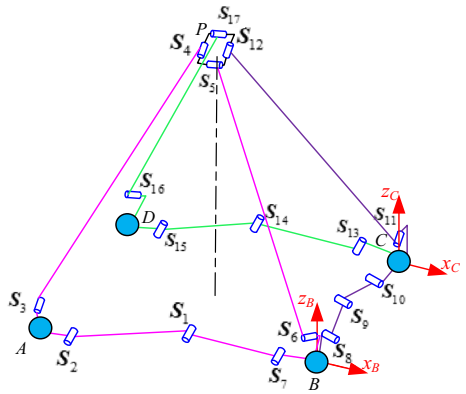

Figure 14 Three-closed-loop mechanism

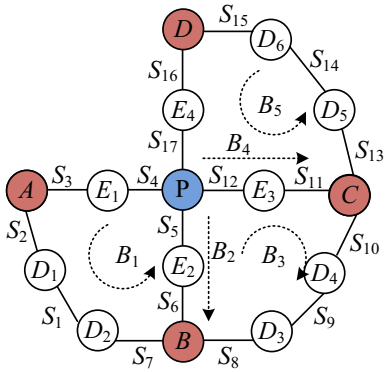

Figure 15 Topology diagram of three-closed-loop mechanism

$\boldsymbol{S}_1$, and $\boldsymbol{S}_7$), and the other is RR ($\boldsymbol{S}_4$, $\boldsymbol{S}_3$), including a two-closed-loop mechanism and a series constraint chain. The two-closed-loop mechanism can also be regarded as a parallel mechanism. The fixed platform (node *B*) and the moving platform (node *P*) are connected by two constraint chains; one is the RR constraint chain ($\boldsymbol{S}_5$, $\boldsymbol{S}_6$), and the other is RRR ($\boldsymbol{S}_8$, $\boldsymbol{S}_9$, and $\boldsymbol{S}_{10}$), including a single closed-loop mechanism ($\boldsymbol{S}_{11}$, $\boldsymbol{S}_{12}$, $\boldsymbol{S}_{17}$, $\boldsymbol{S}_{16}$, $\boldsymbol{S}_{15}$, $\boldsymbol{S}_{14}$, $\boldsymbol{S}_{13}$) and a series constraint chain. The single closed-loop mechanism can also be regarded as a parallel mechanism, and the fixed platform (node *C*) and the moving platform (node *P*) are connected by two constraint chains. One is the RR constraint chain ($\boldsymbol{S}_{11}$, $\boldsymbol{S}_{12}$), and the other is the RRRRR constraint chain ($\boldsymbol{S}_{13}$, $\boldsymbol{S}_{14}$, $\boldsymbol{S}_{15}$, $\boldsymbol{S}_{16}$, $\boldsymbol{S}_{17}$). Firstly, the DOF of the single closed-loop mechanism is analyzed, and a reference coordinate system o_C-$x_Cy_Cz_C$ is established at the center of node *C*. The x_C-axis is along the *DC* line, the z_C-axis is perpendicular to the plane of *ABCD*, and the y_C-axis is determined by the right-hand rule. The kinematic screws of the constraint chains RR and RRRRR in the reference coordinate system are expressed as:

$$\begin{cases} \$^C_{m13} = \begin{pmatrix} 0 & b_{13} & c_{13} & 0 & -x_{13}c_{13} & x_{13}b_{13} \end{pmatrix}^{\mathrm{T}}, \\ \$^C_{m14} = \begin{pmatrix} 0 & b_{13} & c_{13} & -b_{13}z_{14} & -x_{14}c_{13} & x_{14}b_{13} \end{pmatrix}^{\mathrm{T}}, \\ \$^C_{m15} = \begin{pmatrix} 0 & b_{13} & c_{13} & 0 & -x_{15}c_{13} & x_{15}b_{13} \end{pmatrix}^{\mathrm{T}}, \\ \$^C_{m16} = \begin{pmatrix} a_{16} & b_{16} & 0 & 0 & 0 & x_{16}b_{16} \end{pmatrix}^{\mathrm{T}}, \\ \$^P_{m17} = \begin{pmatrix} a_{16} & b_{16} & 0 & -b_{16}z_{17} & a_{16}z_{17} & x_{17}b_{16} - a_{16}y_{17} \end{pmatrix}^{\mathrm{T}}, \end{cases} \tag{4}$$

$$\begin{cases} \$^C_{m11} = \begin{pmatrix} a_{11} & b_{11} & 0 & 0 & 0 & 0 \end{pmatrix}^{\mathrm{T}}, \\ \$^C_{m12} = \begin{pmatrix} a_{11} & b_{11} & 0 & -b_{11}z_{12} & a_{11}z_{12} & x_{12}b_{11} - a_{11}y_{12} \end{pmatrix}^{\mathrm{T}}, \end{cases} \tag{5}$$

where $\begin{pmatrix} a_i & b_i & c_i \end{pmatrix}$ refers to the direction vector of $\boldsymbol{S}_i$, and $\begin{pmatrix} x_i & y_i & z_i \end{pmatrix}$ refers to the position vector of the center of $\boldsymbol{S}_i$ in the reference coordinate system.

Calculate the reciprocal screw of Eqs. (4) and (5), respectively, and the constraint screw applied to *P* can be expressed as:

$$\$^P_{r1} = \begin{pmatrix} 0 & 0 & 0 & -b_{16}c_{13} & a_{16}c_{13} & -a_{16}b_{13} \end{pmatrix}^{\mathrm{T}}, \tag{6}$$

$$\begin{cases} \$^P_{r2} = \begin{pmatrix} 0 & 0 & 0 & 0 & 0 & 1 \end{pmatrix}^{\mathrm{T}}, \\ \$^P_{r3} = \begin{pmatrix} 0 & 0 & 0 & b_{11} & -a_{11} & 0 \end{pmatrix}^{\mathrm{T}}, \\ \$^P_{r4} = \begin{pmatrix} a_{11} & b_{11} & 0 & 0 & 0 & 0 \end{pmatrix}^{\mathrm{T}}, \\ \$^P_{r5} = \begin{pmatrix} x_{12} & y_{12} & z_{12} & 0 & 0 & 0 \end{pmatrix}^{\mathrm{T}}, \end{cases} \tag{7}$$

where $\$^P_{r1}$ represents the constraint couple perpendicular to the revolute joint in the constraint chain ($\boldsymbol{S}_{13}$, $\boldsymbol{S}_{14}$, $\boldsymbol{S}_{15}$, $\boldsymbol{S}_{16}$, $\boldsymbol{S}_{17}$); $\$^P_{r2}$ represents the constraint couple along the *z*-axis; $\$^P_{r3}$ represents the constraint couple parallel to the *xy* plane; $\$^P_{r4}$ represents the constraint force parallel to the axis of the revolute joint at both ends of the link E_3 through the origin of the coordinate system, and $\$^P_{r5}$ represents the constraint force along the axis of the link E_3 through the origin of the coordinate system.

Taking the union of Eqs. (6) and (7) and solving its reciprocal screw, the kinematic screw of *P* relative to *C* can be expressed as:

$$\$^C_{mP} = \begin{pmatrix} 0 & 0 & 0 & -b_{11} & a_{11} & \frac{x_{12}b_{11} - y_{12}a_{11}}{z_{12}} \end{pmatrix}^{\mathrm{T}}. \tag{8}$$

Therefore, the single closed-loop mechanism ($\boldsymbol{S}_{11}$, $\boldsymbol{S}_{12}$, $\boldsymbol{S}_{17}$, $\boldsymbol{S}_{16}$, $\boldsymbol{S}_{15}$, $\boldsymbol{S}_{14}$, $\boldsymbol{S}_{13}$) can be replaced by the generalized translational joint represented by $\$^C_{mP}$. In the closed-loop mechanism ($\boldsymbol{S}_5$, $\boldsymbol{S}_6$, $\boldsymbol{S}_8$, $\boldsymbol{S}_9$, $\boldsymbol{S}_{10}$, $\$^C_{mP}$), node *B* is the fixed platform, node *P* is the moving platform, and a reference coordinate system is established at the center of the fixed platform. The kinematic screws of the constraint chains RR ($\boldsymbol{S}_5$, $\boldsymbol{S}_6$) and RRRP ($\boldsymbol{S}_8$, $\boldsymbol{S}_9$, $\boldsymbol{S}_{10}$, $\$^C_{mP}$) are represented in the reference coordinate system, respectively:

$$\begin{cases} \$_{m5}^{B} = \left(a_5 \;\; b_5 \;\; 0 \;\; -b_5 z_5 \;\; a_5 z_5 \;\; x_5 b_5 - a_5 y_5 \right)^{\mathrm{T}}, \\ \$_{m6}^{B} = \left(a_5 \;\; b_5 \;\; 0 \;\; 0 \;\; 0 \;\; 0 \right)^{\mathrm{T}}, \end{cases} \tag{9}$$

$$\begin{cases} \$_{m8}^{B} = \left(a_8 \;\; b_8 \;\; c_8 \;\; y_8 c_8 \;\; -x_8 c_8 \;\; x_8 b_8 - a_8 y_8 \right)^{\mathrm{T}}, \\ \$_{m9}^{B} = \left(a_8 \;\; b_8 \;\; c_8 \;\; y_9 c_8 - b_8 z_9 \;\; a_8 z_9 - x_9 c_8 \;\; x_9 b_8 - a_8 y_9 \right)^{\mathrm{T}}, \\ \$_{10}^{B} = \left(a_8 \;\; b_8 \;\; c_8 \;\; y_{10} c_8 \;\; -x_{10} c_8 \;\; x_{10} b_8 - a_8 y_{10} \right)^{\mathrm{T}}, \\ \$_{mP}^{B} = \left(0 \;\; 0 \;\; 0 \;\; -b_{11} \;\; a_{11} \;\; \frac{x_{12} b_{11} - y_{12} a_{11}}{z_{12}} \right)^{\mathrm{T}}. \end{cases} \tag{10}$$

Calculate the reciprocal screw of Eqs. (9) and (10) respectively, and the constraint screw applied to P can be expressed as:

$$\begin{cases} \$_{r6}^{P} = \left(0 \;\; 0 \;\; 0 \;\; 0 \;\; 0 \;\; 1 \right)^{\mathrm{T}}, \\ \$_{r7}^{P} = \left(0 \;\; 0 \;\; 0 \;\; b_5 \;\; -a_5 \;\; 0 \right)^{\mathrm{T}}, \\ \$_{r8}^{P} = \left(a_5 \;\; b_5 \;\; 0 \;\; 0 \;\; 0 \;\; 0 \right)^{\mathrm{T}}, \\ \$_{r9}^{P} = \left(x_5 \;\; y_5 \;\; z_5 \;\; 0 \;\; 0 \;\; 0 \right)^{\mathrm{T}}, \end{cases} \tag{11}$$

$$\begin{cases} \$_{r10}^{P} = \left(0 \;\; 0 \;\; 0 \;\; -\frac{c_8}{a_8} \;\; 0 \;\; 1 \right)^{\mathrm{T}}, \\ \$_{r11}^{P} = \left(0 \;\; 0 \;\; 0 \;\; -\frac{b_8}{a_8} \;\; 1 \;\; 0 \right)^{\mathrm{T}}. \end{cases} \tag{12}$$

Taking the union of Eqs. (11) and (12) and solving its reciprocal screw, the kinematic screw of P relative to B can be expressed as:

$$\$_{mP}^{B} = \left(0 \;\; 0 \;\; 0 \;\; -b_5 \;\; a_5 \;\; \frac{x_5 b_5 - a_5 y_5}{z_5} \right)^{\mathrm{T}}. \tag{13}$$

Therefore, the single closed-loop mechanism ($\boldsymbol{S}_5$, $\boldsymbol{S}_6$, $\boldsymbol{S}_8$, $\boldsymbol{S}_9$, $\boldsymbol{S}_{10}$, $\$_{mP}^{C}$) can be replaced by the generalized translational joint represented by $\$_{mP}^{C}$. In the closed-loop mechanism ($\boldsymbol{S}_4$, $\boldsymbol{S}_3$, $\boldsymbol{S}_2$, $\boldsymbol{S}_1$, $\boldsymbol{S}_7$, $\$_{mP}^{C}$), with node B as the fixed platform, node A as the moving platform, the kinematic screw of constraint chains RRR ($\boldsymbol{S}_2$, $\boldsymbol{S}_1$, $\boldsymbol{S}_7$) and RRP ($\boldsymbol{S}_3$, $\boldsymbol{S}_4$, $\$_{mP}^{C}$) are represented respectively in the reference coordinate system:

$$\begin{cases} \$_{m2}^{B} = \left(0 \;\; b_2 \;\; c_2 \;\; 0 \;\; -x_2 c_2 \;\; x_2 b_2 \right)^{\mathrm{T}}, \\ \$_{m1}^{B} = \left(0 \;\; b_2 \;\; c_2 \;\; -b_2 z_1 \;\; -x_1 c_2 \;\; x_1 b_2 \right)^{\mathrm{T}}, \\ \$_{m7}^{B} = \left(0 \;\; b_2 \;\; c_2 \;\; 0 \;\; -x_7 c_2 \;\; x_7 b_2 \right)^{\mathrm{T}}, \end{cases} \tag{14}$$

$$\begin{cases} \$_{m3}^{B} = \left(a_3 \;\; b_3 \;\; 0 \;\; 0 \;\; 0 \;\; x_3 b_3 - y_3 a_3 \right)^{\mathrm{T}}, \\ \$_{m4}^{B} = \left(a_3 \;\; b_3 \;\; 0 \;\; -b_3 z_4 \;\; a_3 z_4 \;\; x_4 b_3 - y_4 a_3 \right)^{\mathrm{T}}, \\ \$_{mP}^{B} = \left(0 \;\; 0 \;\; 0 \;\; -b_5 \;\; a_5 \;\; \frac{x_5 b_5 - a_5 y_5}{z_5} \right)^{\mathrm{T}}. \end{cases} \tag{15}$$

According to Eqs. (14) and (15), the constraint screw applied to node A can be obtained as:

$$\begin{cases} \$_{r12}^{A} = \left(0 \;\; 0 \;\; 0 \;\; 1 \;\; 0 \;\; 0 \right)^{\mathrm{T}}, \\ \$_{r13}^{A} = \left(0 \;\; 0 \;\; 0 \;\; 0 \;\; -b_2 \;\; b_2 \right)^{\mathrm{T}}, \\ \$_{r14}^{A} = \left(0 \;\; b_2 \;\; c_2 \;\; 0 \;\; 0 \;\; 0 \right)^{\mathrm{T}}, \end{cases} \tag{16}$$

$$\begin{cases} \$_{r15}^{A} = \left(0 \;\; 0 \;\; 0 \;\; 0 \;\; 0 \;\; 1 \right)^{\mathrm{T}}, \\ \$_{r16}^{A} = \left(0 \;\; 0 \;\; 0 \;\; -\frac{b_3}{a_3} \;\; 1 \;\; 0 \right)^{\mathrm{T}}, \\ \$_{r17}^{A} = \left(\frac{B}{b_5} \;\; \frac{A b_5}{a_5 z_4 b_3 - a_3 z_4 b_5} \;\; 1 \;\; \frac{y_3 a_3 - x_3 b_3}{a_3} \;\; 0 \;\; 0 \right)^{\mathrm{T}}, \end{cases} \tag{17}$$

where $A = x_4 b_3 - y_4 a_3 - x_3 b_3 + y_3 a_3 - b_3 z_4 C / b_5$, $B = C - \left(b_5 a_5 \left(x_4 b_3 - y_4 a_3 - x_3 b_3 + y_3 a_3 \right) - a_5 b_3 z_4 C \right) / \left(a_3 z_4 b_5 - a_5 b_3 z_4 \right)$, $C = \left(x_5 b_5 - a_5 y_5 \right) / z_5$.

Taking the union of Eqs. (16) and (17) and solving its reciprocal screw, the kinematic screw of A relative to B can be expressed as:

$$\$_{mA}^{B} = \left(0 \;\; 0 \;\; 0 \;\; 1 \;\; 0 \;\; 0 \right)^{\mathrm{T}}. \tag{18}$$

This screw represents movement along the x_C-axis. Similarly, it can be concluded that D also has a DOF of movement along the DC relative to C. In the single closed-loop mechanism ($\boldsymbol{S}_5$, $\boldsymbol{S}_6$, $\boldsymbol{S}_8$, $\boldsymbol{S}_9$, $\boldsymbol{S}_{10}$, $\$_{mP}^{C}$), taking B as the fixed platform and C as the moving platform, using the screw theory, it can be found that C has only one DOF of movement along the BC relative to B. Therefore, considering the removed RRR ($\boldsymbol{S}_{18}$, $\boldsymbol{S}_{19}$, $\boldsymbol{S}_{20}$), the pyramid mechanism can be equivalent to the mechanism shown in Figure 16. The DOF of the mechanism is one.

To sum up, the 4RRR-4RR pyramid unit mechanism is a single DOF overconstrained mechanism, and only one actuation is needed to realize the synchronous folding movement of the four nodes on the bottom with the same pose.

4 Structural Design and Experimental Research of Deployable Mechanism Based on 4RRR-4RR Unit

4.1 Structural Design of Critical Components

The detailed structure design of the mechanism is the key to simulation analysis and experimental research.

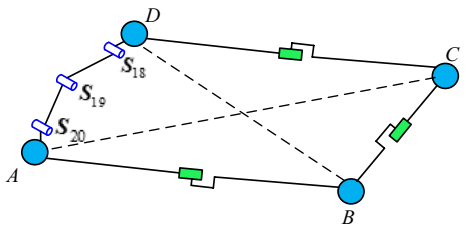

Figure 16 Schematic diagram of the equivalent mechanism of pyramid unit

(a) Central node on reflecting surface (b) Boundary node on reflecting surface (c) Node on back surface

Figure 17 Structural diagram of floral nodes

Figure 18 Connection between components

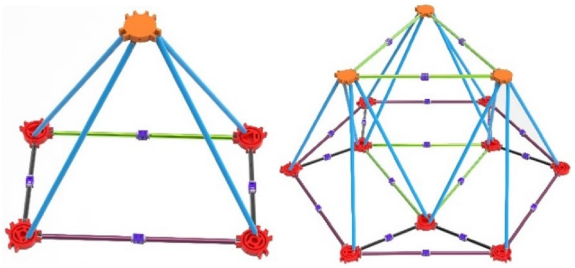

(a) Pyramid basic unit (b) Combination unit

Figure 19 Three-dimensional model of pyramid unit and its combination unit

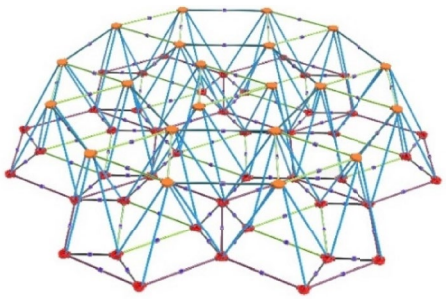

(a) Axonometric view

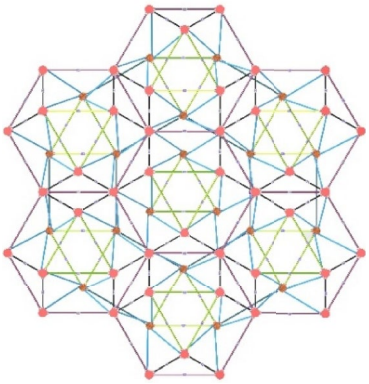

(b) Top view

Figure 20 Three-dimensional model of the expansion unit

The deployable mechanism based on the 4RRR-4RR pyramid comprises floral nodes, synchronous links, web links, synchronous hinges, and other main components. As the critical node of networking, the floral node is connected with 4–7 members, so the structure design of the floral node is complicated. In detailed structural design, on the premise of ensuring the definite movement of the mechanism, the shape of parts should be designed to avoid interference in the folding process of the mechanism. In addition, it is necessary to improve the design practicality and aesthetics of the mechanism as much as possible and reduce the structure's weight. According to the above requirements, the structure of various types of floral nodes is shown in Figure 17, and the components are connected by revolute joints (Figure 18).

Based on the structural design of critical components, the components assemble according to the sketch line model, and finally, the pyramid unit and its combination unit mechanism are obtained (Figure 19). The combination unit is expanded in the form of a circular array to an expansion unit mechanism composed of 7 combination units (Figure 20). Further expansion, the sizeable deployable array mechanism formed by the networking of 31 combination units is shown in Figure 21.

Considering that the lightweight of the large deployable mechanism is realized through the default combination unit, the lightweight combination unit is obtained by default of a group of combination units in the center of the deployable unit (Figure 22), and the large lightweight deployable mechanism is obtained by using the lightweight combination unit as the module (Figure 23).

The component number of the four mechanisms, including the basic unit, combination unit, expansion unit, and array unit, is listed in Table 2. The component number of the pyramid units is small. Due to the expansion of the basic unit, the components number of combination units and expansion units increases, especially the total component number of array units increases sharply to 1737, and the number of revolute joints increases sharply to 3233. This increase in the number of components is also the inevitable result of the large-scale deployable mechanism.

In Table 2, the γ represents the lightweight degree of the mechanism, $\gamma = w_2/(w_1 + w_2) \times 100\%$. The γ of the expansion unit is 10.43%, and the γ of the array unit can reach 18.25%. It can be concluded that it is efficient

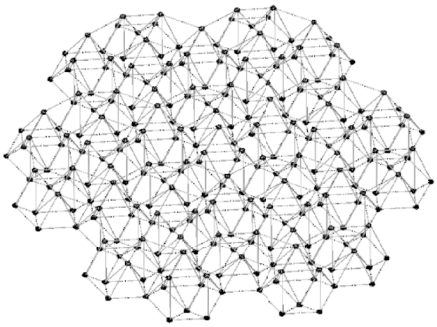

(a) Axonometric view

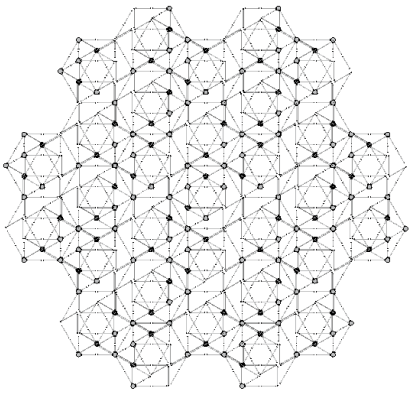

(b) Top view

Figure 21 Three-dimensional model of the large deployable mechanism

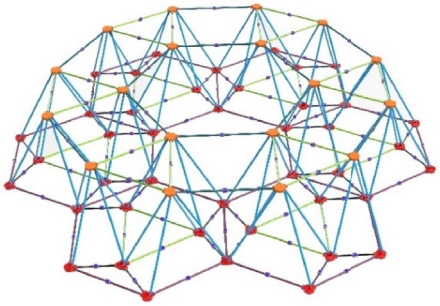

(a) Axonometric view

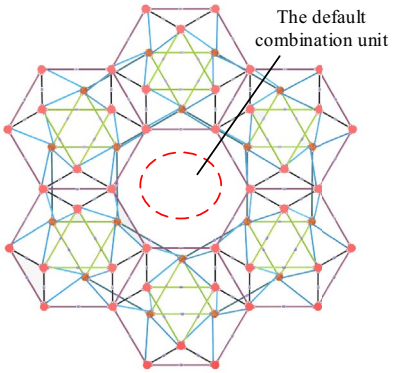

(b) Top view

Figure 22 Three-dimensional model of lightweight expansion unit mechanism

to realize the lightweight of the mechanism by using the default combination unit, and the γ increases with the increase of the size of the deployable mechanism.

4.2 Kinematics Simulation Analysis

The three-dimensional principle model of the expansion unit (Figure 24) is established, and the ADAMS software is used to simulate and analyze the mechanism motion principle, and verify the correctness of the mechanism configuration synthesis design. Perform singularity avoidance processing on the three-dimensional model. All synchronization links of the mechanism are folded at the same small angle, and regenerate the assembly model in this state (Figure 25). Select the synchronous hinges (M_1, M_2, and M_3) at three symmetrical positions on the reflecting surface, and the step actuation functions, which is Step(time, 0, 0 d, 5, 69.4 d), are added. The simulation time is set to 5 s and the step size to 0.25. The expansion unit mechanism moves through the middle folding configuration (Figure 26) to the final folding configuration (Figure 27).

The angle and angular velocity at M_1, M_2, and M_3 actuations are shown in Figure 28. Five types of typical position floral nodes in Figure 24 are selected. The velocity and acceleration of the floral nodes are measured, as shown in Figure 29. According to the simulation results, the expansion mechanism completes the folding movement from 0 s to 5 s. During the movement, the speed first increases and decreases, and the acceleration shows small fluctuation, which can be attributed to the fact that the deployable mechanism is a multi-closed-loop coupling mechanism, and its motion process is extremely complex. When using software for motion simulation, there will be instantaneous velocity fluctuations, but the fluctuation value is small (<0.7), which can be considered reasonable.

The folding model and fully expanded model of the pyramid unit, combination unit, and expansion unit mechanism are shown in Figure 30. The deployable characteristics of these three mechanisms are analyzed quantitatively.

The deployable mechanism presents a cone-shaped platform structure in both an entirely unfolding state and folding state. The ratio of the space volume occupied by the two-state structures is the deployable rate, that is:

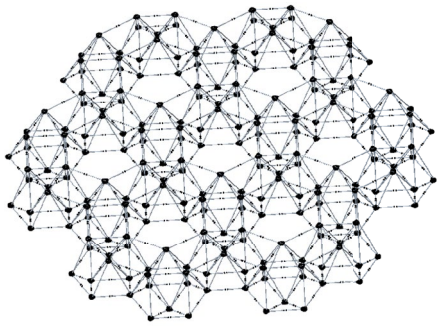

(a) Axonometric view

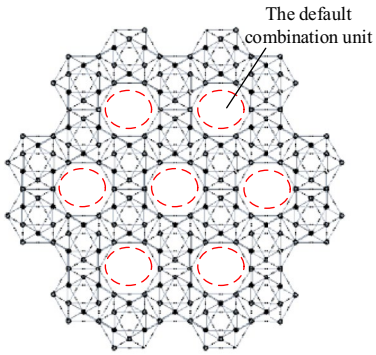

(b) Top view

Figure 23 Three-dimensional model of the large lightweight deployable mechanism

$$\lambda_k = V_j / V_i, \left(i = 1,3,5; j = 2,4,6; k = 1,2,3\right), \quad (19)$$

where V_i(i=1,3,5) and V_j(j=2,4,6) respectively represent the space volume occupied by the mechanism in folding and expanded state of the basic unit, combination unit and expansion unit, and λ_k(k=1,2,3) represent the deployable rate of the basic unit, combination unit and expansion unit.

$$V_i = \frac{1}{3}h_i\left(\frac{\pi d_i^2}{4} + \sqrt{\frac{\pi d_i^2}{4}\cdot\frac{\pi D_i^2}{4}} + \frac{\pi D_i^2}{4}\right), (i = 1,3,5), \quad (20)$$

where h_i(i=1,3,5) represents the total height of the basic unit, combination unit and expansion unit in the folding state, respectively; d_i(i=1,3,5) represents the circumscribed circle diameter of the top node in the folding state of the basic unit, combination unit and expansion unit, respectively; D_i(i=1,3,5) represents the circumscribed circle diameter of the bottom node in the folding state of the basic unit, combination unit and expansion unit, respectively.

$$V_j = \frac{1}{3}h_j\left(\frac{\pi d_j^2}{4} + \sqrt{\frac{\pi d_j^2}{4}\cdot\frac{\pi D_j^2}{4}} + \frac{\pi D_j^2}{4}\right), \left(j = 2,4,6\right), \quad (21)$$

where h_j(j=2, 4, 6) represents the total height of the expanded state of the basic unit, the combination unit and the expansion unit, respectively; d_j(j=2, 4, 6) represents the circumscribed circle diameter of the

Table 2 Components number of large lightweight deployable mechanism

Type of deployable mechanism	Basic unit	Combination unit	Expansion unit	Array unit
Deployable mechanism graphic	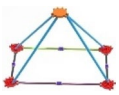	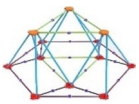	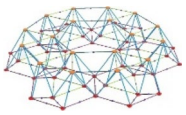	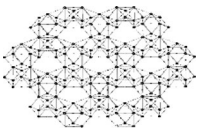
Number of revolute joint	20	76	486	3233
Number of top floral node	1	3	18	66
Number of bottom floral node *A*	2	3	18	66
Number of bottom floral node *B*	2	6	22	76
Number of web link	4	12	72	264
Number of long link	4	24	134	476
Number of short link	4	12	72	264
Number of gears engaged	4	18	114	417
Number of auxiliary connecting link	–	–	24	108
Total number of solid part	21	78	474	1737
Weight of mechanism w_1(kg)	0.76	2.28	12.80	46.60
Default partial weight w_2(kg)	–	–	1.49	10.40
Weight reduction rate γ	–	–	10.43%	18.25%

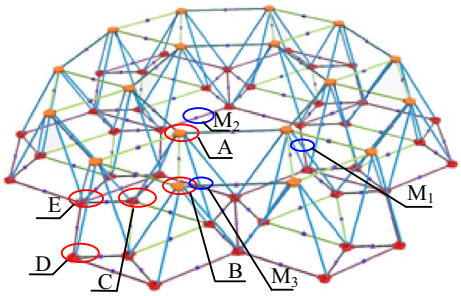

Figure 24 Typical floral node position of the expansion unit

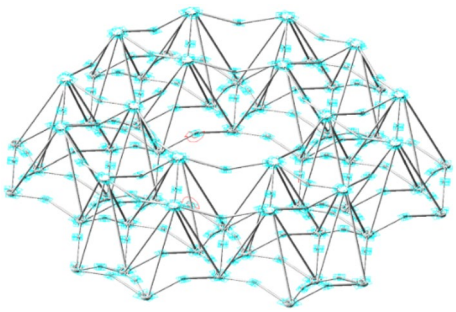

Figure 25 Initial simulation model

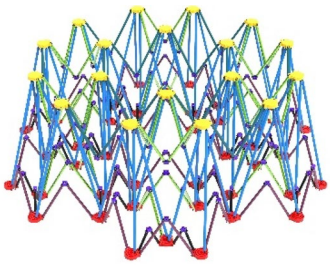

Figure 26 Middle folding model of the expansion unit

(a) Axonometric view (b) top view

Figure 27 Folding model of the expansion unit

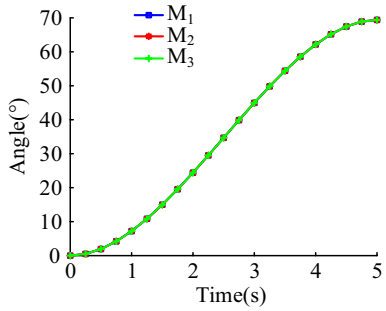

(a) Angle

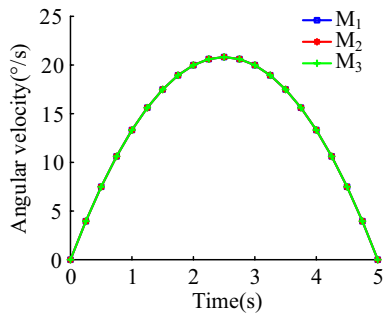

(b) Angular velocity

Figure 28 Angle and angular velocity of actuation

top node in the expanded state of the basic unit, the combination unit and the expansion unit, respectively; $D_j(j=2, 4, 6)$ represents the circumscribed circle diameter of the bottom node in the expanded state of the basic unit, the combination unit and the expansion unit, respectively.

The structural parameters of the basic unit, combination unit, and expansion mechanism are shown in Table 3. According to Eq. (19), the deployable rates of the three mechanisms are 6.67, 9.89, and 12.46, respectively. It is inferred that the deployable rate increases with the size of the deployable mechanism.

4.3 Principle Prototype and its Deployable Experiment

The principle prototypes of the pyramid basic unit and its combination unit mechanism are developed, and deployable experimental research is carried out. Due to

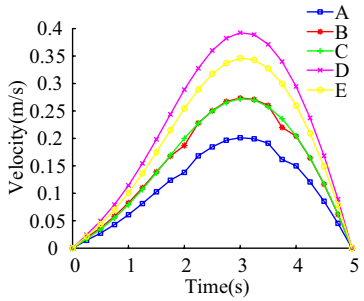

(a) Velocity of five types of floral nodes

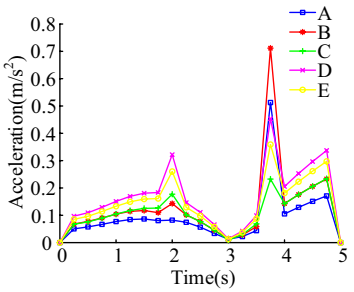

(b) Acceleration of five types of floral nodes

Figure 29 Velocity and acceleration of floral node of the expansion unit

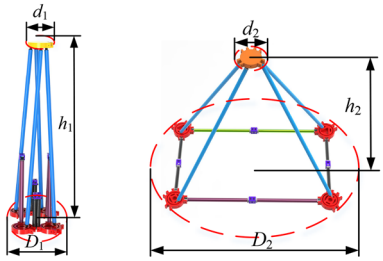

(a) Pyramid unit

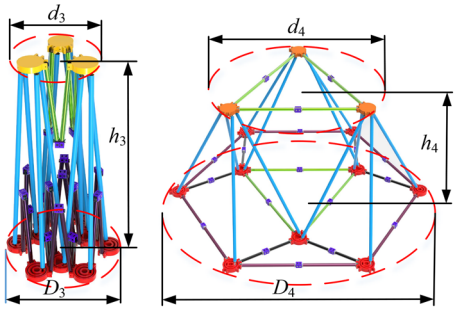

(b) Combination unit

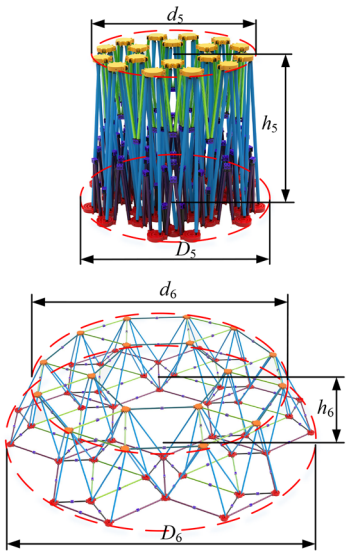

(c) Expansion unit

Figure 30 Folding and unfolding of three mechanisms

the complex structure and non-standard parts of the floral node, 3D printing technology with high precision is used to realize the production of the physical object (Figure 31). To reduce the weight of the mechanism, both web links and synchronous links adopt light carbon fiber links. The experimental prototype of the assembled pyramid basic unit and its combination unit mechanism is shown in Figure 32.

Because of the obstacles such as friction and gravity in the ground experiment, the redundant actuation method is adopted to improve the deployable reliability of the mechanism; that is, torsional springs are added to all synchronous hinges. When the torsional spring is released, the three mechanisms can be expanded from the folding state to the entirely unfolding state. This verifies the expandability of the pyramid unit and its combination unit mechanism.

5 Conclusions

(1) According to the folding principle of the basic unit, a novel pyramid basic deployable unit with good composability and deployability is synthesized by adding the constraint chain method. Taking the regular hexagonal unit as the target, the hexagonal combination unit and its large aperture deployable mechanism are obtained.

(2) The DOF of the pyramid basic unit is one with folding by using the screw theory and the link dismantling method. The detailed structural design of the pyramid unit, the expansion unit, and its array unit mechanism are completed, and the simulation anal-

Table 3 Structural parameters and deployable rate of three mechanisms

Type of deployable mechanism	Basic unit	Combination unit	Expansion unit
h_i(mm)	581.0	577.2	582.0
d_i(mm)	61.0	203.8	580.3
D_i(mm)	224.3	308.4	716.0
h_j(mm)	515.0	515.0	515.0
d_j(mm)	61.0	638.3	2142.7
D_j(mm)	712.8	1061.1	2706.8
V_i(mm^3)	$3.3\pi\times10^6$	$9.6\pi\times10^6$	$6.1\pi\times10^7$
V_j(mm^3)	$2.2\pi\times10^7$	$9.5\pi\times10^7$	$7.6\pi\times10^8$
λ_k	6.67	9.89	12.46

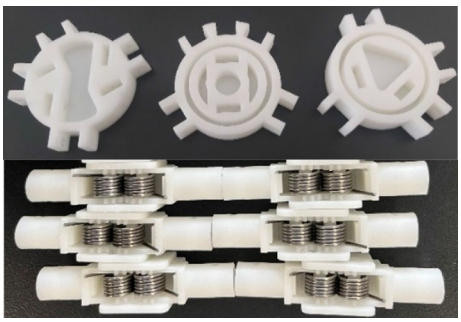

Figure 31 Floral nodes and synchronous hinges

ysis of the folding motion of the three types of units is realized by using ADAMS. The simulation results show that the three mechanisms can realize the unfolding and folding motion, the weight reduction rate and deployable rate of the expansion unit are 10.43% and 12.46 respectively. The weight reduction rate of the array unit mechanism is as high as 18.25%.

(3) The pyramid unit prototype and combination unit prototype are developed, and the prototypes realize the movement from the folding state to the entirely unfolding state under the torsional spring actuation, which verifies the correctness of the configuration synthesis of the truss deployable mechanism based on the pyramid. The work of this paper not only provides a new supporting mechanism for the truss antenna, but also provides a reference for the configuration design of the antenna mechanism with a larger aperture and ultra-lightweight.

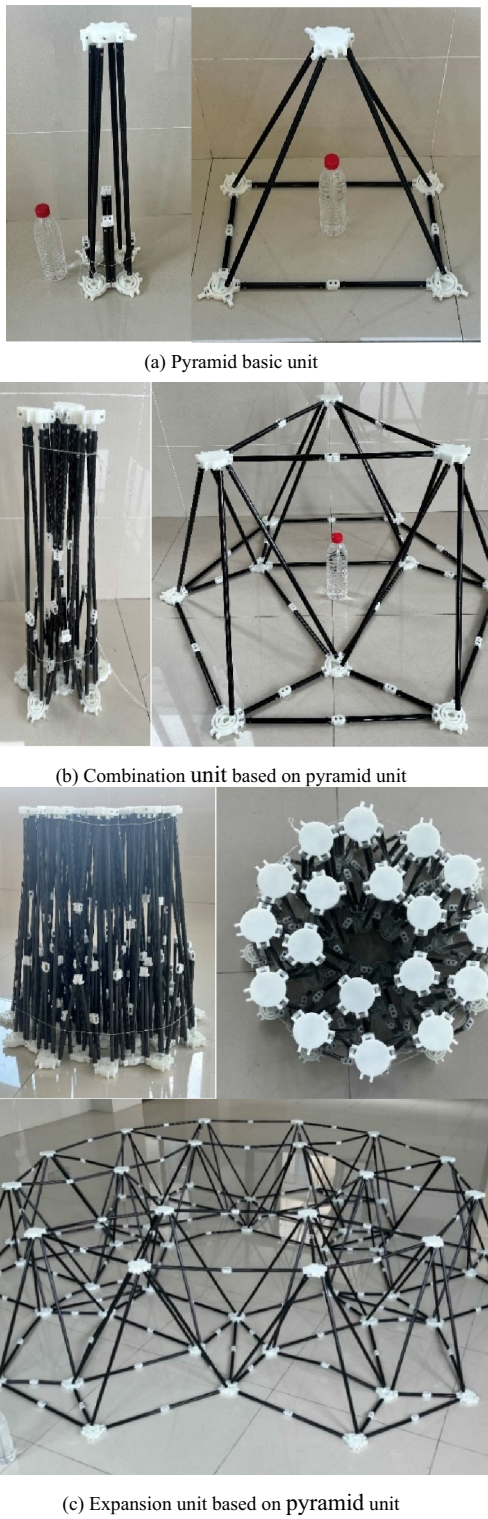

Figure 32 Experiment of folding and unfolding state of the deployable mechanism

Acknowledgements
Not applicable.

Author Contributions
YZ and YX were in charge of the whole trial; JG was responsible for the planning of the content and theoretical analysis; JH performed the structural design and experimental research; GZ analyzed the research on the current situation of the manuscript and contributed in writing. All authors read and approved the final manuscript.

Author's information
Jinwei Guo, born in 1991, is currently a lecturer at *School of Mechanical Engineering, Jiangsu University of Science and Technology, China*. She received her PhD degree in mechatronics engineering from *School of Mechanical Engineering, Yanshan University, China*, in 2021. Her research interests include parallel mechanism theory, spatial deployable mechanism design and analysis
Jianliang He, born in 1995 is currently a postgraduate at School of Mechanical Engineering, Jiangsu University of Science and Technology, China.
Guoxing Zhang, born in 1990 is currently a lecturer at *School of Mechanical Engineering, Jiangsu University of Science and Technology, China*. He received the PhD degree in mechatronics engineering from *School of Mechanical Engineering, Yanshan University, China*, in 2021. His research interests include theory and application of parallel mechanism, research and development of special equipment for marine engineering.
Yongsheng Zhao, is currently a Professor with the *Department of Mechatronics Engineering, School of Mechanical Engineering, Yanshan University, China*. His research interests include parallel mechanism theory and application, spatial deployable mechanism design and application, aerospace equipment and mechatronics systems, and advanced manufacturing technology.
Yundou Xu, is currently a Professor with the *Department of Mechatronics Engineering, School of Mechanical Engineering, Yanshan University, China*. He received the PhD degree in mechatronics engineering from the *School of Mechanical Engineering, Yanshan University, China*, in 2012. His research interests include parallel mechanism theory and application, forging manipulators and deployable antenna mechanism theory and application.

Funding
Supported by National Natural Science Foundation of China (Grant No. 52075467), Jiangsu Provincial Natural Science Foundation of China (Grant No. BK20220649), Natural Science Foundation of the Jiangsu Higher Education Institutions of China (Grant No. 23KJB460010), and Jiangsu Provincial Key R&D Project(Grant No. BE2022062).

Declarations

Competing Interests
The authors declare no competing financial interests.

Received: 26 October 2022 Revised: 9 August 2023 Accepted: 11 August 2023
Published online: 12 September 2023

References

[1] X F Ma, T J Li, J Y Ma, et al. Recent advances in space-deployable structures in China. *Engineering*, 2022, 17(10): 207-219.
[2] D Zou, G Liu, Z Rao, et al. Design of vibration energy harvesters with customized nonlinear forces. *Mechanical Systems and Signal Processing*, 2021, 153: 107526.
[3] K Wang, J Zhou, H Ouyang, et al. A dual quasi-zero-stiffness sliding-mode triboelectric nanogenerator for harvesting ultralow-low frequency vibration energy. *Mechanical Systems and Signal Processing*, 2021, 151: 107368.
[4] X F Ma, Y Li, T J Li, et al. Design and analysis of a novel deployable hexagonal prism module for parabolic cylinder antenna. *Mechanical Sciences*, 2021, 12(1): 9-18.
[5] P Cheng, H F Ding, W A Cao, et al. A novel family of umbrella-shaped deployable mechanisms constructed by multi-layer and multi-loop spatial linkage units. *Mechanism and Machine Theory*, 2021, 161: 104169.
[6] R W Liu, H W Guo, R Q Liu, et al. Structural design and optimization of large cable–rib tension deployable antenna structure with dynamic constraint. *Acta Astronautica*, 2018, 151: 160-172.
[7] X Z Qi, H L Huang, B Li, et al. A large ring deployable mechanism for space satellite antenna. *Aerospace Science and Technology*, 2016, 58: 498-510.
[8] Y X Yang, L Liu, J L Li, et al. Featured services and performance of BDS-3. *Science Bulletin*, 2021, 66(20): 2135-2143.
[9] X J Li, Q Y Meng, X F Gu, et al. A hybrid method combining pixel-based and object-oriented methods and its application in Hungary using Chinese HJ-1 satellite images. *International Journal of Remote Sensing*, 2013, 34(13): 4655-4668.
[10] M C Phocas, E G Christoforou, P Dimitriou. Kinematics and control approach for deployable and reconfigurable rigid bar linkage structures. *Engineering Structures*, 2020, 208: 110310.
[11] Z H Sun, Y Q Zhang, D W Yang. Structural design, analysis, and experimental verification of an H-style deployable mechanism for large space-borne mesh antennas. *Acta Astronautica*, 2021, 178: 481-498.
[12] Y Chen, Z You. On mobile assemblies of Bennett linkage. *Proceedings of the Royal Society A: Mathematical, Physical and Engineering Sciences*, 2008, 464(2093): 1275-1293.
[13] D C Hofmann, P Bordeenithikasem, Z Dawson, et al. Investigating bulk metallic glasses as ball-and-cone locators for spacecraft deployable structures. *Aerospace Science and Technology*, 2018, 82: 513-519.
[14] Q Z Meng, X J Liu, F G Xie. Structure design and kinematic analysis of a class of ring truss deployable mechanisms for satellite antennas based on novel basic units. *Mechanism and Machine Theory*, 2022, 174: 104881.
[15] C Yang, B Wang, S C Zhong, et al. On tailoring deployable mechanism of a bistable composite tape-spring structure. *Composites Communications*, 2022, 32: 101171.
[16] Z J Chen, C Shi, H W Guo, et al. Design and accuracy analysis of a new high-rigidity modular planar deployable antenna mechanism. *Engineering Structures*, 2022, 253: 113770.
[17] L Y Guo, Y S Zhao, S C Lu, et al. A novel spatial support mechanism for planar deployable antennas. *Acta Astronautica*, 2021, 188: 479-490.
[18] S N Lyu, P F Yao, H Xiao, et al. Approximating cylinders with bundle-folding plane-symmetric Bricard linkages. *International Journal of Mechanical Sciences*, 2022, 221: 107231.
[19] S Wang, Y H Gao, H L Huang, et al. Design of deployable curved-surface rigid origami flashers. *Mechanism and Machine Theory*, 2022, 167: 104512.
[20] K A Takamatsu, J Onoda. New deployable truss concepts for large antenna structures or solar concentrators. *Journal of Spacecraft and Rockets*, 1991, 28(3): 330-338.
[21] D K Tian, H M Gao, L Jin, et al. Design and kinematic analysis of a multi-fold rib modular deployable antenna mechanism. *Mechanical Sciences*, 2022, 13(1): 519-533.
[22] R G Wang, J X Sun, J S Dai. Design analysis and type synthesis of a petal-inspired space deployable-foldable mechanism. *Mechanism and Machine Theory*, 2019, 141: 151-170.
[23] H Huang, F L Guan, L L Pan, et al. Design and deploying study of a new petal-type deployable solid surface antenna. *Acta Astronautica*, 2018, 148: 99-110.
[24] H Huang, Q Cheng, L Zheng, et al. Development for petal-type deployable solid-surface reflector by uniaxial rotation mechanism. *Acta Astronautica*, 2021, 178: 511-521.
[25] F Y Wu, Y Yu, Y J Zhao, et al. Nonlinear dynamics analysis of flexible deployable linkage mechanisms using the finite particle method. *International Journal of Structural Stability and Dynamics*, 2021, 21(13): 2150184.
[26] G X Zhang, D H Zheng, J W Guo, et al. Dynamic modeling and mobility analysis of the 3-R(RRR)R+R antenna mechanism. *Robotica*, 2021, 39(8): 1485-1503.
[27] Y D Xu, L L Chen, W L Liu, et al. Type synthesis of the deployable mechanisms for the truss antenna using the method of adding constraint chains. *Journal of Mechanisms and Robotics*, 2018, 10(4): 041002.
[28] J W Guo, Y S Zhao, G X Zhang, et al. Configuration synthesis and unfolding stiffness characteristics analysis of a truss antenna connecting

mechanism based on URU-RR-URU hexagonal deployable unit. *Mechanism and Machine Theory*, 2022, 177: 105047.
[29] J W Guo, Y S Zhao, Y D Xu, et al. Mechanics analysis and structural design of a truss deployable antenna mechanism based on 3RR-3URU tetrahedral unit. *Mechanism and Machine Theory*, 2022, 171: 104749.
[30] J W Guo, Y S Zhao, Y D Xu, et al. A novel modular deployable mechanism for the truss antenna: Assembly principle and performance analysis. *Aerospace Science and Technology*, 2020, 105: 105976.
[31] S R Kim, D Y Lee, S J Ahn, et al. Morphing origami block for lightweight reconfigurable system. *IEEE Transactions on Robotics*, 2020, 37(2): 494-505.
[32] Q J Ze, S Wu, J Z Dai, et al. Spinning-enabled wireless amphibious origami millirobot. *Nature Communications*, 2022, 13(1): 3118.
[33] A Y N Sofla, D M Elzey, H N G Wadley. Shape morphing hinged truss structures. *Smart Materials and Structures*, 2009, 18(6): 065012.
[34] L Dai, F L Guan, J K Guest. Structural optimization and model fabrication of a double-ring deployable antenna truss. *Acta Astronautica*, 2014, 94(2): 843-851.
[35] L Dai, R Xiao. Optimal design and analysis of deployable antenna truss structure based on dynamic characteristics restraints. *Aerospace Science and Technology*, 2020, 106: 106086.
[36] C Wang, J L Li, D W Zhang. Optimization design method for kirigami-inspired space deployable structures with cylindrical surfaces. *Applied Mathematical Modelling*, 2021, 89: 1575-1598.
[37] Y D Xu, Y Zhao, Y Yue, et al. Type synthesis of overconstrained 2R1T parallel mechanisms with the fewest kinematic joints based on the ultimate constraint wrenches. *Mechanism and Machine Theory*, 2020, 147: 103766.
[38] B Mei, F G Xie, X J Liu, et al. Elasto-geometrical error modeling and compensation of a five-axis parallel machining robot. *Precision Engineering*, 2021, 69: 48-61.